

Transport and noise properties of a normal metal–superconductor–normal metal junction with mixed singlet and chiral triplet pairings

Ganesh C. Paul,^{1,*} Paramita Dutta,^{1,†} and Arijit Saha^{1,‡}

¹*Institute of Physics, Sachivalaya Marg, Bhubaneswar-751005, India*

We study transport and zero frequency shot noise properties of a normal metal-superconductor-normal metal (NSN) junction, with the superconductor having mixed singlet and chiral triplet pairings. We show that in the subgapped regime when the chiral triplet pairing amplitude dominates over that of the singlet, a resonance phenomena emerges out at zero energy where all the quantum mechanical scattering probabilities acquire a value of 0.25. At the resonance, crossed Andreev reflection mediating through such junction, acquires a zero energy peak. This reflects as a zero energy peak in the conductance as well depending on the doping concentration. We also investigate shot noise for this system and show that shot noise cross-correlation is negative in the subgapped regime when the triplet pairing dominates over the singlet one. The latter is in sharp contrast to the positive shot noise obtained when the singlet pairing is the dominating one.

PACS numbers: 74.45.+c, 73.63.-b, 74.20.Rp, 74.40.De

I. INTRODUCTION

Study of transport signatures at the interface of normal metal-superconductor (NS) hybrid structures has been the subject of intense research interest during the last few decades^{1–3}. The key issue behind the low-energy quantum transport phenomena in this type of hybrid junction is the process of Andreev reflection⁴. When a normal metal electron with energy below the superconducting gap regime incident on the NS interface, a hole with opposite spin reflects back from the interface and as a result a Cooper pair jumps into the superconductor. Such reflection process is called the phenomenon of Andreev reflection (AR)⁴ in literature.

Another intriguing phenomenon occurs in case of a normal metal-superconductor material-normal metal (NSN) junction in which an electron incident from one of the normal metal leads forms a pair with another electron from the other normal metal lead and jumps into the superconductor as a Cooper pair. Such non-local process is called crossed Andreev reflection (CAR)^{5–10} whose signature has been verified in various experiments^{11–18}. CAR can also be used to produce non local entangled electron pairs^{7,9,19}. From the practical point of view, superconducting hybrid structures can be designed by placing a bulk superconducting material in close proximity to a normal metal system^{11–13,17,18} and superconducting correlation is actually induced into the non-superconducting region via the proximity effect.

Till date, most of the research works have been carried out using either conventional spin-singlet^{3,5} or spin-triplet^{20–22} superconductor with the orbital even and odd parity, respectively. Nevertheless this classification of the superconductors holds as long as they maintain inversion symmetry²³. A different situation arises when we consider an unconventional superconductor without inversion symmetry. The physical properties of such superconductors with broken inversion symmetry becomes interesting due to the mixing of spin-singlet and spin-triplet

order parameter without any parity symmetry. Non-centrosymmetric superconductors^{24,25} (NCS) are examples of such superconductors where the spin-singlet and triplet pairing mixing²⁶ is present with time reversal symmetry but with broken inversion symmetry^{27–29}. The absence of the parity symmetry in NCS may lead to several interesting properties determined by the ratio of the amplitudes of the spin-singlet to spin-triplet pair potentials³⁰. Among such properties emergence of topological spin current in NCS superconductor^{31,32}, magnetoelectric effects²³, magnetism²⁵ etc. have been reported in recent times. These interesting properties have drawn attention of the community towards exploring the nature of NCS superconductor and as a consequence, the list of NCS materials is growing gradually³³. Another reason behind this attraction is that recently, it has been shown that this type of superconductor characterized by time-reversal symmetry can hold an even number of Majorana Fermions^{34–36}. Therefore, further investigations are required to explore the properties of NCS as well as the effect of NCS on transport phenomena through superconducting hybrid junctions.

Very recently transport signature of NS and superconductor-normal metal-superconductor (SNS) junction with mixed singlet and chiral triplet pairing has been reported by Burset *et al.*³⁰. They obtain a zero-energy peak in the conductance in a NS junction when the triplet pairing is the dominating one over the singlet part. However, NSN junction and the properties of CAR in the above context has never been studied so far. The latter motivated us to investigate transport and shot noise phenomena through a NSN junction in which a one-dimensional (1D) nanowire (NW) is placed in close proximity to a superconductor which contains a pair potential of mixed singlet and chiral triplet type. The NW is attached to two normal metal (N) leads. We incorporate three regimes corresponding to the amplitude of the spin-singlet part being lesser, equal to and larger than that of the spin-triplet part. We

adopt Blonder-Tinkham-Klapwijk (BTK) formalism¹ to calculate the quantum mechanical scattering amplitudes through the junction and conductance, shot noise therein. We find zero-energy peak in the conductance depending on the degree of mixing of the pair potentials and the doping. We also calculate the zero frequency shot noise (auto and cross-correlation) and show that the shot noise cross-correlation becomes positive to negative as long as the triplet pairing dominates over the singlet one.

The remainder of this paper is organized as follows. In Sec. II we describe our model. Sec. III is devoted to the scattering matrix (BTK) formalism by which we calculate the quantum mechanical scattering amplitudes to obtain conductance and shot noise through the NSN junction. We present our numerical results in Sec. IV which includes scattering probabilities, conductance and shot noise for different parameter regimes. Finally, we summarize and conclude in Sec. V.

II. MODEL

In Fig. 1 we present the schematic of our proposed set-up in which a 1D NW is placed in close proximity to a bulk superconducting material. Here superconductivity is induced in the NW via the proximity effect. The NW is attached to two normal metal leads. A gate voltage G can tune the chemical potential inside the NW. Instead of

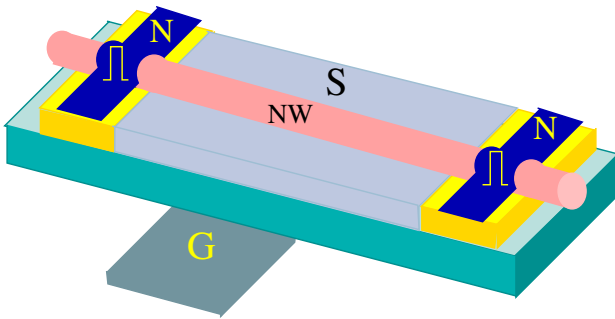


FIG. 1. (Color online) Schematic of the quasi one-dimensional NSN setup in which a nanowire (NW) (pink, light grey) is placed in close proximity to a bulk superconductor (light brown, light grey) and superconductivity is induced in the NW via the proximity effect. The NW is attached to two normal (N) metal leads (blue, black). The gate G (light cyan, light grey) controls the chemical potential in the NW. Two δ -function barriers are symbolically denoted by the two yellow (light grey) rectangular barriers at each N-NW interface.

conventional s-wave superconductor here we consider the pairing potential of the superconductor as a combination of spin-singlet and chiral spin-triplet states. We choose the x -axis along the direction of the NW. The two N-NW interfaces are located at $x = 0$ and $x = L$ respectively. At each N-NW interface we consider an insulating barrier which is modeled by the δ -function potential given

as $V(x) = (\hbar^2 k_F/m)Z\delta(x)$ where k_F is the Fermi wave vector, m denotes electron mass and Z is the strength of the barrier.

Hence the NSN junction can be described by the Bogoliubov-deGennes (BdG) equations as,

$$H(\mathbf{k})\psi(\mathbf{k}) = \epsilon\psi(\mathbf{k}) \quad (1)$$

where

$$H(\mathbf{k}) = \begin{bmatrix} [E(\mathbf{k}) - \mu]\hat{\sigma}_0 & \hat{\Delta}(\mathbf{k}) \\ \hat{\Delta}^\dagger(\mathbf{k}) & [\mu - E(-\mathbf{k})]\hat{\sigma}_0 \end{bmatrix}. \quad (2)$$

Here $E(\mathbf{k}) = (\hbar^2/2m)k_x^2 + U$ is the dispersion relation of the electronic excitation measured from chemical potential μ . U is the electrostatic potential in the normal region. $\hat{\sigma}_0$ is the 2×2 Identity matrix in spin space. We write the four component wave function in Nambu representation as $\psi(\mathbf{k}) = [u_\uparrow(\mathbf{k}), u_\downarrow(\mathbf{k}), v_\uparrow(\mathbf{k}), v_\downarrow(\mathbf{k})]^T$ where $u_\sigma(\mathbf{k})$ and $v_\sigma(\mathbf{k})$ are the electron and hole components respectively with spin $\sigma = \uparrow, \downarrow$ and \mathbf{k} is the wave vector.

In the superconducting region, due to the presence of both spin-singlet and chiral spin-triplet states, the pairing potential $\hat{\Delta}(\mathbf{k})$ (2×2 matrix) can be written in general $\hat{\Delta}(\mathbf{k}) = i[\Delta_s(\mathbf{k})\hat{\sigma}_0 + \sum_{j=1}^3 d_j(\mathbf{k})\hat{\sigma}_j]\hat{\sigma}_2 e^{i\phi}$. Here, $\hat{\sigma}_{1,2,3}$ are Pauli spin matrices operating on spin space and ϕ is the superconducting phase factor. The spin singlet pairing $\Delta_s(\mathbf{k})$ characterizes the conventional s wave superconducting order parameter. Here we consider only the mean-field value of $\Delta_s(\mathbf{k})$ i.e. $\Delta_s(\mathbf{k}) = \Delta_s$. On the contrary, triplet pairing potential is described by an odd vector function as $\mathbf{d}(\mathbf{k}) = -\mathbf{d}(-\mathbf{k})$.

Following Burset *et al.*³⁰ we take chiral triplet state of the form,

$$\begin{aligned} \mathbf{d}(\mathbf{k}) &= \Delta_p \frac{k_x + i\chi k_y}{|\mathbf{k}|} \hat{z} \\ &= \Delta_p e^{i\chi\theta} \hat{z}, \end{aligned} \quad (3)$$

where Δ_p is non-negative amplitude of the triplet pairing potential. χ determines the orientation of the angular momentum of the Cooper pairs and it can take \pm sign corresponding to the parallel and anti-parallel direction respectively. θ represents the relative orientation between the singlet and chiral triplet pairing states. With this consideration paring potential now takes the form, $\hat{\Delta}(\mathbf{k}) = i[\Delta_s\hat{\sigma}_0 + \Delta_p e^{i\chi\theta}\hat{\sigma}_3]\hat{\sigma}_2 e^{i\phi}$. This simple choice of the pairing potential takes into consideration the mixing of the spin-singlet and spin-triplet states. With this pairing potential, the band dispersion becomes³⁰

$$\epsilon_{1,2}(\mathbf{k}) = \sqrt{E^2(\mathbf{k}) + \Delta_s^2 + \Delta_p^2 \pm 2\Delta_s\Delta_p \cos\theta}, \quad (4)$$

which explicitly depends on the relative orientation of singlet and chiral triplet pairing components. Now the full 4×4 Hamiltonian $H(\mathbf{k})$ can be written in block diagonal form which implies decoupling of two spin channels $\uparrow\downarrow$ and $\downarrow\uparrow$. Hence the effective pairing potentials corresponding to these two channels become³⁰

$$\Delta_{1,2}(\theta) = [\Delta_s \pm \Delta_p e^{i\chi\theta}]\hat{\sigma}_2 e^{i\phi}. \quad (5)$$

Therefore, it will now be sufficient to consider two effective complex pair potentials $\Delta_{1,2}(\theta)$ among which $\Delta_2(\theta)$ vanishes for a particular choice of the $\Delta_s (= \Delta_p \cos \theta)$ and also it changes sign for $\Delta_s > \Delta_p$.

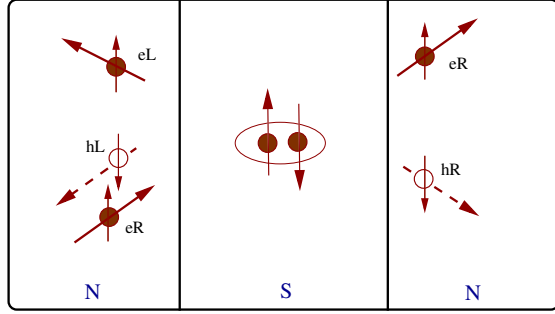


FIG. 2. (Color online) Schematic for the electron (solid sphere) and hole (hollow sphere) trajectories (solid and dashed lines, respectively) corresponding to the four quantum mechanical scattering processes occurring at a NSN junction. Notations in the figure denote eR: right-moving electron; eL: left-moving electron; hR: right-moving hole; hL: left-moving hole.

In the quasi 1D limit, electrons can propagate only in the x -direction with the transverse component of the wave vector k_y being conserved. Hence the band energy $E(\pm \mathbf{k})$ can be written as $E(\pm k_x)$ for a particular choice of k_y . We choose $k_y = 0$ for our analysis. Also, we assume that the band energies for the electrons moving to the left and right are equal to each other. We define right movers by $\theta^+ = \theta$ and left movers by $\theta^- = \pi - \theta$. After decoupling for each spin channel, the BdG equations in the 2×2 form can be written as,

$$\begin{bmatrix} [E(\alpha \mathbf{k}) - \mu] & s_\sigma \Delta_\sigma(\theta^\alpha) e^{i\phi} \\ s_\sigma \Delta_\sigma^*(\theta^\alpha) e^{-i\phi} & [\mu - E(-\alpha \mathbf{k})] \end{bmatrix} \begin{bmatrix} u_\sigma(\theta^\alpha) \\ v_\sigma(\theta^\alpha) \end{bmatrix} = \epsilon \begin{bmatrix} u_\sigma(\theta^\alpha) \\ v_\sigma(\theta^\alpha) \end{bmatrix} \quad (6)$$

where $\epsilon \geq 0$ is the excitation energy; $\alpha = \pm$ corresponds to the right and left movers; $s_\sigma = (-1)^{\sigma-1}$ and $\sigma = 1, 2$ denotes the different spin channels. Thus, the pairing potential is different for each independent spin channel as well as for direction of motion of particles. Also, the gap amplitude can be different depending on the direction of motion as argued in Ref. 2. Left mover with spin \uparrow and \downarrow will be effected by the pairing potential $\Delta_1(\theta^-)$ and $-\Delta_2(\theta^-)$ respectively. On the other hand, right mover will experience the effective pairing potential $\Delta_1(\theta^+)$ and $-\Delta_2(\theta^+)$ corresponding to \uparrow and \downarrow spin channels respectively.

Electron and hole components of the wave functions are given by,

$$u_\sigma(\theta^\alpha) = \frac{1}{\sqrt{2}} \left(1 + \frac{\sqrt{\epsilon^2 - |\Delta_\sigma(\theta^\alpha)|^2}}{\epsilon} \right), \quad (7)$$

$$v_\sigma(\theta^\alpha) = \frac{1}{\sqrt{2}} \left(1 - \frac{\sqrt{\epsilon^2 - |\Delta_\sigma(\theta^\alpha)|^2}}{\epsilon} \right). \quad (8)$$

III. THE SCATTERING MATRIX

In this section we present the scattering matrix obtained employing the BTK formalism¹ for our NSN geometry. Normal metallic region is described by considering $\Delta(\mathbf{k}) = 0$ and also we set $U = 0$ there to carry out our analysis. When an incident electron coming from one of the normal metal leads with energy below the superconducting gap scatters from the NS interface, the corresponding scattering phenomena can be described by four possible quantum mechanical processes. These processes are: (a) normal reflection of electron from the NS boundary (b) AR of incident electron as a hole in the same lead (c) elastic co-tunneling (CT) in which the incident electron transmits to the other lead as an electron and (d) transmission of hole in the other lead via the CAR process. The schematic of these processes are displayed in Fig 2.

In order to obtain reflection, AR, CT and CAR amplitudes through the NSN junction we write the wave functions in the three regions as follow,

$$\begin{aligned} \psi_\sigma^L(x) &= e^{ik_e x} \begin{bmatrix} 1 \\ 0 \end{bmatrix} + r_\sigma(\epsilon) e^{-ik_e x} \begin{bmatrix} 1 \\ 0 \end{bmatrix} \\ &\quad + r_{h\sigma}(\epsilon) e^{ik_h x} \begin{bmatrix} 0 \\ 1 \end{bmatrix}, \end{aligned} \quad (9)$$

$$\begin{aligned} \psi_\sigma^S(x) &= a_\sigma(\epsilon) e^{iq_e x} \begin{bmatrix} u_\sigma(\theta^+) e^{i\phi} \\ \eta_\sigma^*(\theta^+) v_\sigma(\theta^+) \end{bmatrix} \\ &\quad + b_\sigma(\epsilon) e^{-iq_e x} \begin{bmatrix} u_\sigma(\theta^-) e^{i\phi} \\ \eta_\sigma^*(\theta^-) v_\sigma(\theta^-) \end{bmatrix} \\ &\quad + c_\sigma(\epsilon) e^{-iq_h x} \begin{bmatrix} \eta_\sigma(\theta^+) v_\sigma(\theta^+) \\ u_\sigma(\theta^+) e^{-i\phi} \end{bmatrix} \\ &\quad + d_\sigma(\epsilon) e^{iq_h x} \begin{bmatrix} \eta_\sigma(\theta^-) v_\sigma(\theta^-) \\ u_\sigma(\theta^-) e^{-i\phi} \end{bmatrix}, \end{aligned} \quad (10)$$

$$\psi_\sigma^R(x) = t_\sigma(\epsilon) e^{ik_e x} \begin{bmatrix} 1 \\ 0 \end{bmatrix} + t_{h\sigma}(\epsilon) e^{-ik_h x} \begin{bmatrix} 0 \\ 1 \end{bmatrix} \quad (11)$$

with $\eta_\sigma(\theta^\alpha) = s_\sigma \Delta_\sigma(\theta^\alpha) / |\Delta_\sigma(\theta^\alpha)|$. Here $\psi_\sigma^L(x)$, $\psi_\sigma^R(x)$, $\psi_\sigma^S(x)$ are the wave functions for the left, right normal metal leads and the superconductor respectively. k_e and k_h are the wave vectors for the electron and hole respectively in the normal metal regions whereas, q_e and q_h are the same for the superconducting region. They can be expressed as,

$$\begin{aligned} k_{e(h)} &= k_F \sqrt{(1 \pm \epsilon/\mu)} \\ q_{e(h)} &= k_F \sqrt{\frac{(\mu + U) \pm i \sqrt{|\Delta_\sigma|^2 - \epsilon^2}}{\mu}} \end{aligned} \quad (12)$$

where, Δ_σ can be Δ_1 or Δ_2 depending on the spin channel.

Here, r_σ , $r_{h\sigma}$, $t_{e\sigma}$ and $t_{h\sigma}$ denote the normal reflection, AR, CT and CAR amplitudes respectively. They can be

obtained by considering the boundary conditions for the wave functions such as, for the left boundary ($x = 0$)

$$\begin{aligned} \psi^L|_{x=0} &= \psi^S|_{x=0}, \\ \partial_x \psi^S|_{x=0} - \partial_x \psi^L|_{x=0} &= k_F Z \psi^L(0) \end{aligned} \quad (13)$$

and for the right boundary ($x = L$),

$$\begin{aligned} \psi^R|_{x=L} &= \psi^S|_{x=L}, \\ \partial_x \psi^R|_{x=L} - \partial_x \psi^S|_{x=L} &= k_F Z \psi^R(L). \end{aligned} \quad (14)$$

Numerically solving these eight equations we get the amplitudes corresponding to all scattering processes (r_σ , $r_{h\sigma}$, $t_{e\sigma}$ and $t_{h\sigma}$) and probability therein. We solve these equations for each spin channel, $\sigma = 1$ and $\sigma = 2$. Here we denote $R_{e\sigma} = |r_\sigma|^2$, $R_{h\sigma} = \frac{k_h}{k_e} |r_{h\sigma}|^2$, $T_{e\sigma} = |t_\sigma|^2$ and $T_{h\sigma} = \frac{k_h}{k_e} |t_{h\sigma}|^2$ as the probability for normal reflection, AR, CT and CAR respectively. All the probabilities together satisfy the unitarity relation,

$$T_{e\sigma} + T_{h\sigma} + R_{e\sigma} + R_{h\sigma} = 1. \quad (15)$$

for each spin channel ($\sigma=1,2$) separately. Note that, the factor k_h/k_e is introduced in order to maintain the probability current conservation.

At zero temperature, conductance for a particular electron energy ϵ and a chiral angle θ can be found by taking contributions from both the spin channel $\sigma = 1$ and 2 using the following relation,

$$G(\epsilon, \theta) = \frac{e^2}{h} \sum_{\sigma} (|t_{e\sigma}|^2 - |t_{h\sigma}|^2). \quad (16)$$

We normalize the conductance by the normal state conductance $G_0 = \frac{2e^2}{h} D(\theta)$, where, $D(\theta) = 4 \cos^2 \theta / (Z^2 + 4 \cos^2 \theta)$ ³⁰.

As θ denotes the relative orientation between the triplet and singlet components of the pairing potential, its range can be $[-\pi/2, \pi/2]$ with respect to the direction of the incoming electron³⁰. Therefore, the angle-averaged conductance can be obtained after integrating $G(\epsilon, \theta)$ over θ as,

$$\tilde{G}(\epsilon) = \int_{-\pi/2}^{\pi/2} G(\epsilon, \theta) \cos \theta \, d\theta. \quad (17)$$

IV. NUMERICAL RESULTS

In this section we present our numerical results for the scattering probabilities, conductance and shot noise. Depending on the ratio of triplet to singlet phase of the superconducting pairing potential we consider three different regimes of interest: $\Delta_p < \Delta_s$, $\Delta_p = \Delta_s$ and $\Delta_p > \Delta_s$. Although we present all our numerical results only for the regime $\Delta_p > \Delta_s$ which is the interesting regime. Also, we show $R_{e\sigma}$, $R_{h\sigma}$, $T_{e\sigma}$ and $T_{h\sigma}$ as functions of different

parameters of the system only for $\sigma = 1$ without loss of generality and hence we use the notation R_e , R_h , T_e and T_h in place of $R_{e\sigma}$, $R_{h\sigma}$, $T_{e\sigma}$ and $T_{h\sigma}$, respectively throughout our results. Length of the superconducting region and energy of the incident electron are normalized by the superconducting coherence length (ξ) and amplitude of the pair potential Δ_0 , respectively *i.e.*, $L/\xi \rightarrow L$, $\epsilon/\Delta_0 \rightarrow \epsilon$. Moreover, depending on the doping in the normal metal side we divide our study into two categories such as, undoped case where we set $\mu = 0$ and finite doping condition for which we fix $\mu = 5$. Throughout our calculation, the values of some parameters are taken as $Z = 2$, $\phi = 0$, $e = 1$, $h = 1$ and $U = 15$ (for the superconducting region). The chosen value of U makes the superconductor doped and creates large Fermi wavelength mismatch between the normal and superconducting regions and also fulfill the requirement of the mean field condition of superconductivity *i.e.* $\mu + U \gg \Delta_0$. We use the unit where $\Delta_0 = 1$.

A. Scattering Processes

In this section we show our numerical results for the scattering probabilities for two different doping conditions.

1. Undoped Regime ($\mu = 0$)

In Fig. 3 we show all the four possible scattering probabilities R_e , R_h , T_e and T_h as a function of the length (L) of the superconductor for $\Delta_p > \Delta_s$ regime, setting incident electron energy $\epsilon = 0$. With this choice of energy value we are within the superconducting sub-gapped regime. Panel (a) and (b) in Fig. 3 correspond to $\theta = 0$ and $\theta = \pi/4$ respectively.

It is evident from Fig. 3(a) that for $\theta = 0$, AR dominates over all other scattering processes except for very small values of L . To illustrate this, we show R_e , R_h , T_e and T_h in the inset of Fig. 3(a), for small values of L ($L \ll \xi$). Note that all the scattering probabilities are almost identical to each other for $L < 0.03\xi$ *i.e.* they occur with almost equal probability of value ~ 0.25 which is in sharp contrast to the $\Delta_s > \Delta_p$ regime where T_h (CAR) is vanishingly small. On the other hand, for $L > 0.075\xi$, all scattering processes except AR become vanishingly small.

To investigate whether the above mentioned resonance phenomena persists for other values of θ , we show the behavior of R_e , R_h , T_e and T_h as a function of L in Fig. 3(b) for $\theta = \pi/4$. Note that the scattering probabilities no longer remain equal to each other for $L \ll \xi$ regime even we set $\Delta_p > \Delta_s$.

Instead, probability for CT dominates over the others and attains the maximum value ~ 1 for $L \ll \xi$ which is illustrated in the inset of Fig. 3(b). Nevertheless, as

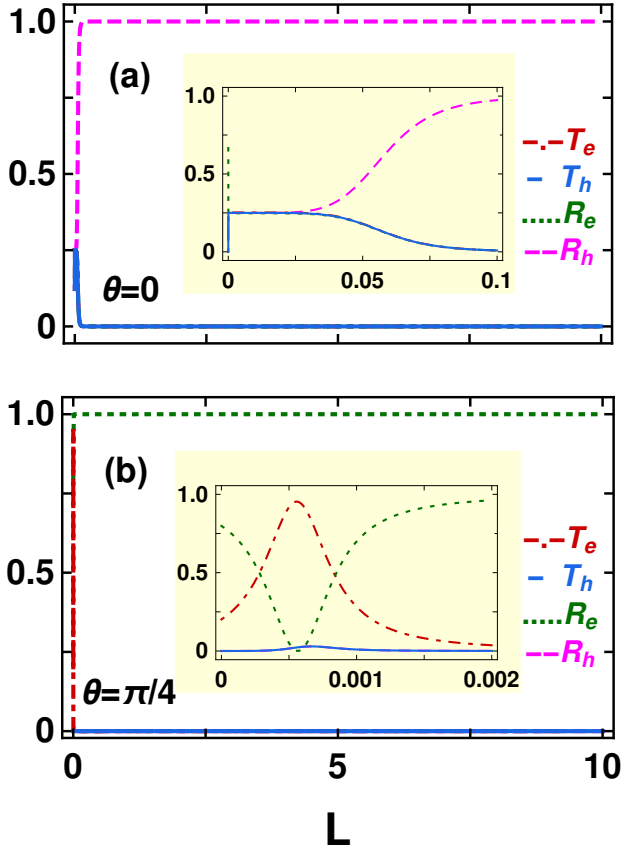


FIG. 3. (Color online) Quantum-mechanical scattering probabilities (normal reflection R_e , Andreev reflection R_h , elastic co-tunneling T_e and crossed Andreev reflection T_h) are plotted as a function of the length (L) of the superconducting region. In the insets, the behavior of the scattering probabilities are shown when $L \ll \xi$. Here $\theta = 0$ in the upper panel and $\theta = \pi/4$ in the lower panel. The value of the other parameters are chosen to be $\mu = 0$, $\Delta_s = 0.25$, $\Delta_p = 0.75$ and $\epsilon = 0$.

soon as L becomes larger than ξ normal reflection begins to dominate over CT as visible from Fig. 3(b). For $L \gg \xi$ all processes except normal reflection die away and the junction becomes perfectly reflecting. Comparing the two cases we can say that for $\theta = 0$, AR dominates over the other processes when $L \gg \xi$. On the other hand, the contribution for normal reflection process becomes dominant for $\theta = \pi/4$ and $L \gg \xi$. For both the θ values, the contribution for the two non-local processes T_e (CT) and T_h (CAR) becomes vanishingly small when $L > \xi$.

We also analyse the dependence of this resonance phenomenon on the incident electron energy and show the corresponding behavior of R_e , R_h , T_e and T_h as a function of ϵ in Fig. 4. It is evident from the inset of Fig. 4(a) that all the scattering probabilities become equal in magnitude (~ 0.25) at $\epsilon = 0$. Similar $1/4$ resonance behavior at finite energy had been predicted earlier in a superconducting double barrier (NSNSN) structure³⁷ where the superconductor was considered to be a purely singlet

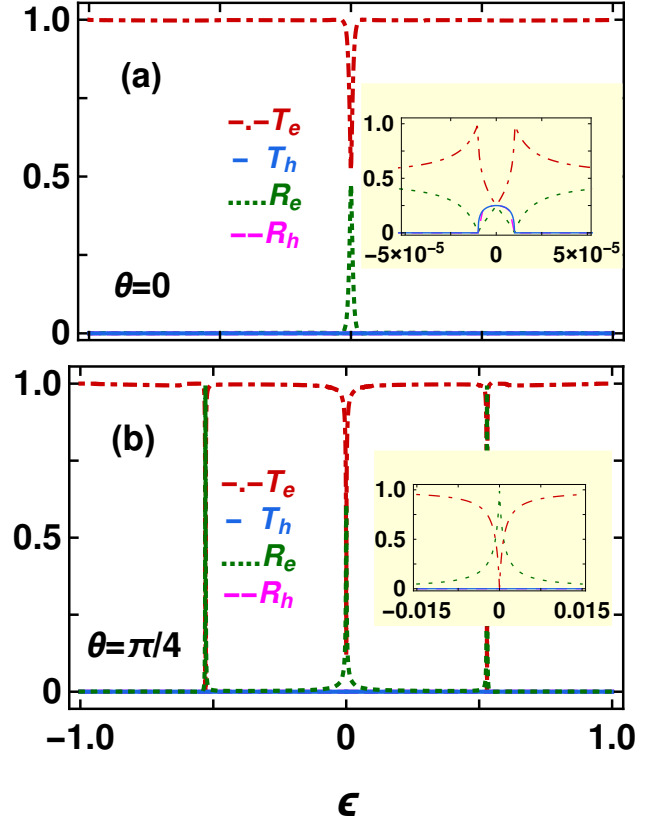


FIG. 4. (Color online) The behavior of normal reflection R_e , Andreev reflection R_h , elastic co-tunneling T_e and crossed Andreev reflection T_h are shown as a function of the energy (ϵ) of the incident electron in the subgapped regime. Here $\theta = 0$ in the upper panel and $\theta = \pi/4$ in the lower panel. We choose $L = 0.003\xi$ and the value of the other parameters are same as in Fig. 3.

one. However, zero energy peak (ZEP) for CAR with peak height of ~ 0.25 for a NSN geometry in the $\Delta_p > \Delta_s$ regime when $\theta = 0$ is one of the main results of our paper. The physical reason behind the emergence of this ZEP can be attributed to the vanishing of the effective pairing gap for $\theta = 0$ when $\Delta_p = \Delta_s$ and changing sign depending on whether $\Delta_p > \Delta_s$ or $\Delta_p < \Delta_s$ (see Eq.(4)). This leads to the appearance of a zero-energy Andreev bound state and zero energy resonance phenomena therein.

On the other hand, the behavior of R_e , R_h , T_e and T_h for $\theta = \pi/4$ is depicted in Fig. 4(b). We observe that normal reflection has sharp zero energy as well as finite energy peaks, while the CT process has sharp dips at those energy values. These peaks are clearly shown in the inset of Fig. 4(b). In this parameter regime AR and CAR probability are always vanishingly small. Note that, for this θ value, the energy dispersion changes according to Eq.(4) leading to different resonance behavior.

Note that the amplitudes for different scattering processes depend on whether $\mu > \epsilon$ or $\mu < \epsilon$. This can be understood qualitatively from Eq. (12). Whether k_p is real or imaginary, it completely depends on the relative

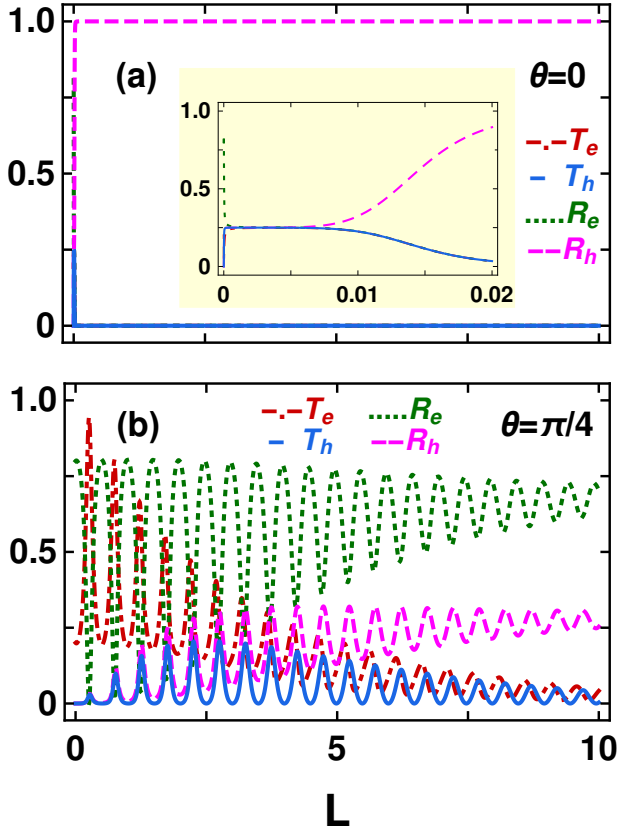


FIG. 5. (Color online) The behavior of quantum-mechanical scattering probabilities (normal reflection R_e , Andreev reflection R_h , elastic co-tunneling T_e and crossed Andreev reflection T_h) are plotted as a function of the length (L) of the superconducting region for the doped regime. Here we have chosen $\mu = 5$, $\Delta_s = 0.25$, $\Delta_p = 0.75$ and $\epsilon = 0$ with $\theta = 0$ (upper panel) and $\pi/4$ (lower panel). In the inset of the upper panel, the behavior of R_e , R_h , T_e and T_h is elaborated when $L \ll \xi$.

strength of gate voltage and applied bias which in turn changes the scattering amplitudes. For $\epsilon > \mu$, particles can only tunnel through the superconductor resulting in $T_e = 1$ as shown in Fig. 4(a) for $\theta = 0$.

The zero energy resonance phenomena also survives with the enhancement of the barrier strength Z . The reason behind such resonance structure and ZEP for the AR and CAR can be attributed to the formation of Andreev bound states (ABS) inside the proximity induced superconducting region of the NW. The nature of the ABS from the shot noise point of view will be presented at a later subsection of this article.

2. Doped Regime ($\mu = 5$)

Here, we examine the behavior of the scattering probabilities with the change of doping in the normal metal while choosing the value of the other parameters same as

in the undoped case. Fig. 5 depicts the variation of T_e , T_h , R_e and R_h as a function of the length of the superconductor where panel (a) and (b) correspond to $\theta = 0$ and $\pi/4$, respectively. In Fig. 5(a) we observe that the behavior of the scattering probabilities qualitatively remains similar to that of the undoped ($\mu = 0$) case. Here also AR dominates over all other scattering processes and also the $1/4$ resonance phenomena takes place below a critical value of L/ξ . The latter is depicted in the inset of Fig. 5(a). Hence, doping has a very small effect on the scattering phenomena when $\theta = 0$ and $\epsilon = 0$.

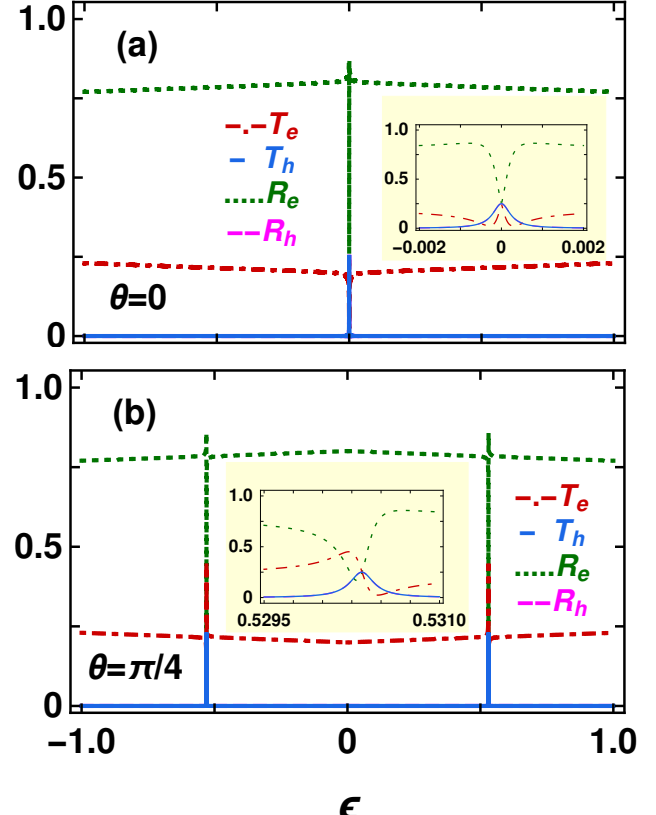


FIG. 6. (Color online) The behavior of R_e , R_h , T_e and T_h is shown as a function of energy of the incident electron in the subgapped regime with $\theta = 0$ (upper panel) and $\theta = \pi/4$ (lower panel). The value of the other parameters are chosen to be the same as in Fig. 5.

However, if we choose a different value of θ , the effect of doping is much more visible in Fig. 5(b) in comparison to Fig. 3(b). All the scattering probabilities become oscillatory with respect to L/ξ when we set $\theta = \pi/4$ for finite doped regime. The only common feature between the two cases is that with the enhancement of the length of the superconducting region, normal reflection dominates over all other processes while CT and CAR become vanishingly small. These periodic variation with L can be manifested as the interference between the electron and hole wave-functions inside the superconducting region.

In Fig. 6 we show the variation of R_e , R_h , T_e and

T_h with incident electron energy ϵ . Here panel (a) and (b) correspond to $\theta = 0$ and $\theta = \pi/4$ while the value of the other parameters remain unchanged as in the undoped case. The inset of Fig. 6(a) illustrates that AR, CAR and CT processes acquire sharp peak and all of them achieve a value ~ 0.25 at zero energy. They gradually become vanishingly small for $|\epsilon| > 0.002\Delta_0$. On the other hand the probability for R_e becomes close to unity and the junction becomes nearly perfectly reflecting for energy values other than zero. On the contrary, for $\theta = \pi/4$, the ZEP no longer exists as depicted in Fig. 6(b). There are two resonance points symmetrically situated around $\epsilon \approx \pm 0.5\Delta_0$ in the subgapped regime. Both AR and CAR have sharp peaks whereas the other two processes (R_e and CT) have dip at those points (see the inset of Fig. 6(b)). These peaks (dips) are shifted from zero energy due to finite θ in the doped regime.

Note that all the results presented here is for symmetric barriers placed at the two N-NW interfaces. However, our results remain qualitatively unchanged even for asymmetric barrier strengths at the two interfaces.

B. Conductance

In this subsection, we study the angle averaged normalized conductance (\tilde{G}/G_0) as a function of incident electron energy ϵ using Eq. (17). The results are presented in Fig. 7 where, panel (a) and (b) correspond to the undoped ($\mu = 0$) and doped ($\mu = 5$) case, respectively. Here we have averaged over all possible orientations between the singlet and triplet pair potentials. For the undoped case, conductance increases almost linearly with energy as shown in Fig. 7(a) irrespective of the ratio of the pairing potential amplitudes. At $\epsilon = 0$, averaged conductance exactly becomes zero for all the three regimes of the pairing potentials. On the contrary, in the doped regime, conductance behavior is non-monotonic. There are peaks at $\epsilon = \pm\Delta_0$ for all the three regimes ($\Delta_p < \Delta_s$, $\Delta_p = \Delta_s$, $\Delta_p > \Delta_s$) and these peaks correspond to the density of states at the two boundaries of the superconducting gap. In the scattering probability profiles we obtain ZEP for CAR and CT processes in the regime $\Delta_p > \Delta_s$. However in the conductance profile, we obtain a ZEP when $\Delta_p = \Delta_s$ for the finite doping condition. There is only finite average conductance (no ZEP) for the other two regimes *i.e.* $\Delta_p < \Delta_s$ or $\Delta_p > \Delta_s$ (see Fig. 7(b))

The absence of the ZEP in the orientation averaged conductance profile corresponding to $\Delta_p > \Delta_s$ regime can be explained as follows. At $\epsilon = 0$, we have zero conductance corresponding to the regime $\Delta_p > \Delta_s$ for the undoped case. This happens because at $\epsilon = 0$ either both CT and CAR probabilities have the same magnitude describing the resonance condition or they are vanishingly small as depicted in Fig. 4[(a)-(b)]. Taking into account contributions due to all possible orientations (θ) between the singlet and triplet pairings we finally obtain zero con-

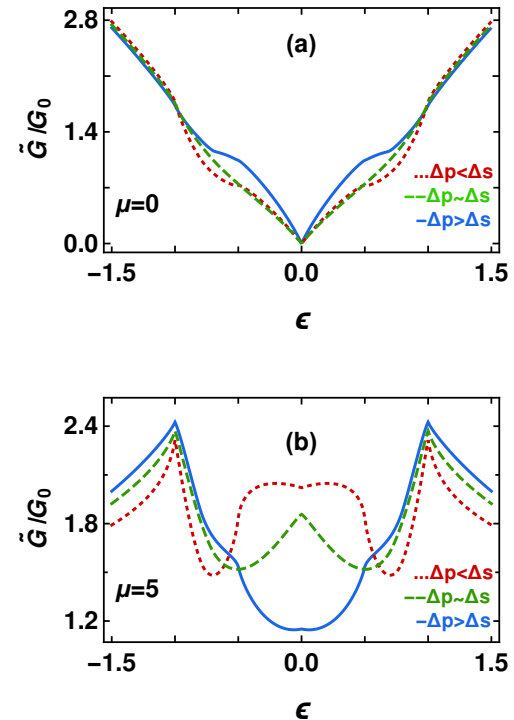


FIG. 7. (Color online) The behavior of normalized conductance (\tilde{G}/G_0) is shown as a function of the energy (ϵ) of the incident electron for three different regime of mixed pairing potential ($\Delta_p < \Delta_s$, $\Delta_p \sim \Delta_s$ and $\Delta_p > \Delta_s$). Here we choose $L = 0.75\xi$. The upper and lower panel correspond to undoped ($\mu = 0$) and doped ($\mu = 5$) regime.

ductance for the undoped case. Although for non-zero ϵ , the contribution in the conductance can arise due to entirely CT (T_e) process whose probability is one for $\epsilon \neq 0$. On the other hand, for the doped case we have finite conductance at $\epsilon = 0$ after averaging over all possible θ s. The reason behind this feature can be attributed to the finite T_e contribution for $\theta = \pi/4$ (see Fig. 6(b)).

C. Shot noise

This sub-section is devoted to explore the shot noise properties mediated through our NSN junction. Our aim is to investigate the nature of zero energy resonance as mentioned before via the noise. In general shot noise in a mesoscopic system arises due to the quantization of the electric charge^{38,39}. Measurement of shot noise can even be utilized to probe the nature of superconducting wavefunction¹³. Here we neglect thermal noise as throughout our calculation we set the temperature to zero.

The correlation function of the current in the two leads labeled by i and j , is defined as³⁸,

$$S_{ij}(t - t') = \langle \Delta \hat{I}_i(t) \Delta \hat{I}_j(t') + \Delta \hat{I}_j(t') \Delta \hat{I}_i(t) \rangle \quad (18)$$

in terms of the operator,

$$\Delta\hat{I}_i(t) = \hat{I}_i(t) - \langle \hat{I}_i(t) \rangle. \quad (19)$$

After performing Fourier transform Eq. (18) becomes,

$$S_{ij}(\omega)\delta(\omega + \omega') = \frac{1}{2\pi} \langle \Delta\hat{I}_i(\omega)\Delta\hat{I}_j(\omega') + \Delta\hat{I}_j(\omega')\Delta\hat{I}_i(\omega) \rangle \quad (20)$$

with

$$\Delta\hat{I}_i(\omega) = \hat{I}_i(\omega) - \langle \hat{I}_i(\omega) \rangle. \quad (21)$$

We find the expression for zero frequency ($\omega = 0$) shot noise cross correlation in terms of the scattering amplitudes following Ref. 40. The general expression for current fluctuation in two different leads i and j in presence of an external bias is given by⁴⁰,

$$S_{ij} = \frac{2e^2}{h} \sum_{k,l \in N,S,\alpha,\beta,\gamma,\delta \in e,h} \text{sgn}(\alpha)\text{sgn}(\beta) \int dE A_{k\gamma,l\delta}(i\alpha, E) A_{l\delta,k\gamma}(j\beta, E) f_{k\gamma}(E) [1 - f_{l\delta}(E)] \quad (22)$$

where $A_{k\gamma,l\delta}(i\alpha, E) = \delta_{ik}\delta_{il}\delta_{\alpha\gamma}\delta_{\alpha\delta} - s_{ik}^{\alpha\gamma\dagger}(E)s_{il}^{\alpha\delta}(E)$. Here $\text{sgn}(\alpha) = +1$ corresponds to $\alpha = e$ (electron) and $\text{sgn}(\alpha) = -1$ refers to $\alpha = h$ (hole). $s_{ik}^{\alpha\gamma}$ represents the scattering amplitude for a particle of type γ incident from lead k being transmitted to lead i as a particle of type α ($\alpha, \gamma \in e, h$). Eq. (22) is valid for current fluctuations in mesoscopic hybrid junctions when the superconductor region is maintained at a fixed potential⁴⁰. Also, we consider zero frequency limit to neglect capacitive component in order to avoid displacement currents due to charging.

It is well known that zero-frequency current fluctuation between two different normal metal leads is always negative for fermions³⁸. Nevertheless in presence of a singlet superconductor shot noise cross-correlation can be positive depending on the parameter values^{13,14,41,42}. The expression for shot noise in terms of transmission and reflection co-efficients are given in the Appendix .

In Fig. 8[(a)-(b)] we show the behavior of shot noise cross correlation (S_{ij}) as a function of the incident electron energy ϵ in the regime $\Delta_p > \Delta_s$ for the undoped ($\mu = 0$) case. Here panel (a) and (b) correspond to $\theta = 0$ and $\theta = \pi/4$ respectively. We observe that S_{ij} gradually reduces to -1 for very small range around $\epsilon = 0$, but sharply reverts back to zero exactly at $\epsilon = 0$ as illustrated by the inset of Fig. 8(a). This sign change of S_{ij} from -1 to 0 reflects the presence of the zero energy resonance where all the scattering probabilities have equal magnitude of 1/4. Moreover, for energy values other than zero below the subgapped regime, S_{ij} is exactly zero since $T_e = 1$ and $R_e = R_h = T_h = 0$ (see Fig. 4(a)). On the other hand, there are sharp positive peaks in the S_{ij} profile for $\theta = \pi/4$, as shown in Fig. 8(b). For $\epsilon = 0$

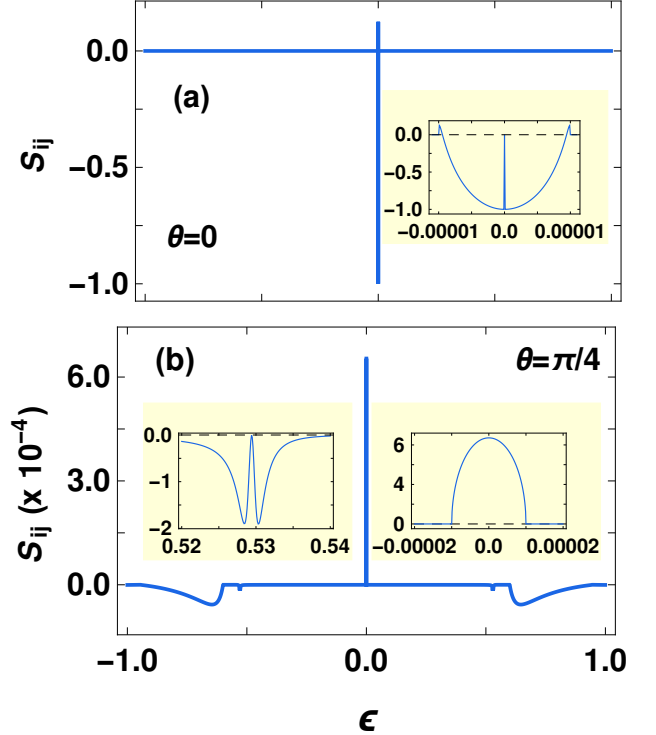


FIG. 8. (Color online) The behavior of shot noise cross-correlation (S_{ij}) is shown as a function of energy (ϵ) of the incident electron. Here $L = 0.003\xi$, $\Delta_s = 0.25$, $\Delta_p = 0.75$ and $\theta = 0$ (upper panel), $\theta = \pi/4$ (lower panel) with $\mu = 0$.

and $\epsilon \approx 0.5$, $R_e = 1$ and $R_h = T_e = T_h = 0$ as depicted in Fig. 4(b). Also $T_e = 1$ for the other values of energy. Hence, shot noise cross correlation S_{ij} is vanishingly small ($\sim 10^{-4}$) compared to the $\theta = 0$ case.

Similar to the undoped case, we also calculate the zero frequency shot noise cross-correlation for the doped system. Our results are shown in Fig. 9[(a)-(b)]. We qualitatively obtain the similar behavior for S_{ij} as in the undoped case. As depicted in Fig. 6(a), at $\epsilon = 0$ all the scattering probabilities have the same value of 0.25 resulting in zero S_{ij} (see Fig. 9(a)). On the other hand, for $\theta = \pi/4$, S_{ij} becomes -1 in a small range of around $\epsilon \approx \pm 0.5\Delta_0$. Another interesting feature is that S_{ij} changes sign from negative to positive for both the cases $\theta = 0$ (around $\epsilon = 0$) and $\theta = \pi/4$ (around $\epsilon \approx \pm 0.5\Delta_0$) as depicted in the insets of Fig. 9(a) and Fig. 9(b) respectively. This transition of the shot noise cross-correlation from negative to positive value is in contrast to that case of purely singlet superconductor where shot noise cross correlation is only positive^{13,14,41}.

So far, the behavior of shot noise cross-correlation has been discussed for particular values of θ which is the orientation between the triplet to singlet amplitude of the superconductor. To obtain the angle averaged shot noise

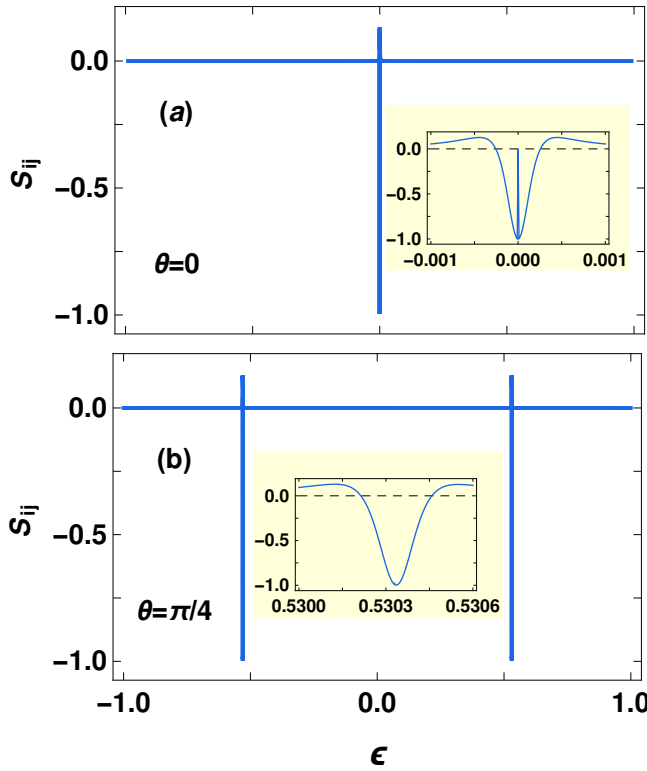


FIG. 9. (Color online) The feature of shot noise cross-correlation (S_{ij}) is depicted as a function of energy (ϵ) of the incident electron. Here $\mu = 5$ and $\theta = 0$ (upper panel) and $\theta = \pi/4$ (lower panel). We choose the value of the other parameters same as in Fig. 8.

we integrate over all possible orientations as,

$$\tilde{S}_{ij} = \int_{-\pi/2}^{\pi/2} S_{ij} \cos \theta \, d\theta. \quad (23)$$

The behavior of angle averaged shot noise \tilde{S}_{ij} is presented as a function of the energy of the incident electron in Fig. 10. For $\mu = 0$, \tilde{S}_{ij} vanishes at $\epsilon = 0$ irrespective of the ratio of the pairing potential amplitudes. Moreover, the feature of \tilde{S}_{ij} is monotonic similar to the conductance (see Fig. 7(a)) for $\epsilon \neq 0$.

On the other hand, there are crossovers from positive to negative and vice-versa for the doped case corresponding to all the three regimes of the pairing amplitudes. Nevertheless, \tilde{S}_{ij} is always negative for $\Delta_p \geq \Delta_s$ in the subgapped regime *i.e.* $\epsilon \leq \Delta_0$. However when the s wave pairing amplitude dominates over that of the p wave ($\Delta_s > \Delta_p$), \tilde{S}_{ij} remains positive over the major range of the subgapped regime and changes sign around $\epsilon \approx 0.75\Delta_0$. The emergence of negative shot noise cross correlation (\tilde{S}_{ij}) in the $\Delta_p \geq \Delta_s$ regime in contrast to the positive \tilde{S}_{ij} in the $\Delta_p < \Delta_s$ regime is another main result of our article.

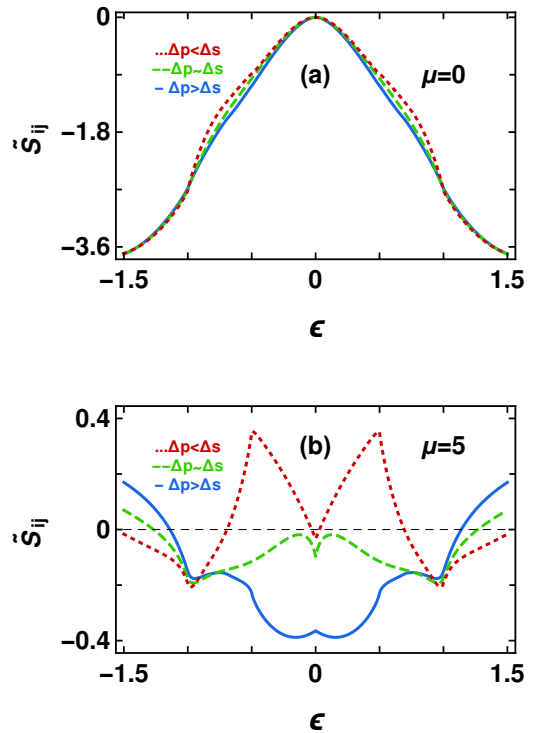


FIG. 10. (Color online) Angle averaged shot noise cross-correlation (\tilde{S}_{ij}) is shown as a function of incident electron energy (ϵ) for three different regimes of mixed pairing potential ($\Delta_p < \Delta_s$, $\Delta_p \sim \Delta_s$ and $\Delta_p > \Delta_s$). We have chosen $L = 0.75\xi$. The upper and lower panel represent $\mu = 0$ and $\mu = 5$ cases respectively.

V. SUMMARY AND CONCLUSIONS

To summarize, we have explored the conductance and shot noise phenomena through a NSN junction where the superconductor is characterized by a mixture of both the spin-singlet and spin-triplet pairings. Our NSN set up comprises of a 1D NW placed in close proximity to a bulk superconductor with mixed pairing of singlet and triplet type (*e.g.* NCS superconductor). The NW is also coupled to two normal metal leads. Depending on the ratio of their pairing amplitudes and the doping concentration in the normal metal region we study the behavior of scattering amplitudes, conductance and zero frequency shot noise for three different regimes ($\Delta_p > \Delta_s$, $\Delta_p = \Delta_s$, $\Delta_p < \Delta_s$). The main feature we obtain in this geometry is the appearance of a zero energy resonance. At the resonance, probability for all the four possible scattering processes (reflection, AR, CT and CAR) acquire same magnitude (1/4) when chiral triplet pairing amplitude dominates over the singlet one. The angle averaged conductance also exhibits a zero energy peak in the doped regime. Moreover, for a chosen orientation (θ) between the singlet and triplet pairing, zero frequency shot noise cross correlation exhibits positive to negative transition

in the chiral triplet pairing dominated regime. However, for the doped regime, angle averaged shot noise remains negative in the subgapped regime when $\Delta_p \geq \Delta_s$ and becomes positive in the opposite regime ($\Delta_s > \Delta_p$). Very recently, transition from positive to negative shot noise cross-correlation also has been reported in the context of Majorana bound states^{43–45}.

As far as practical realization of our NSN structure is concerned, a NW may be possible to fabricate in close proximity to a NCS superconductor for *e.g.* Mo₃Al₂C, BiPd etc.^{33,46}. Such superconductors posses a coherence length $\xi \approx 10 - 20$ nm for critical magnetic field $H_{c2}(0) \approx 1.2 - 1.5$ T as reported in Ref. 33 and 46. Hence, our findings for the angle averaged conductance and shot noise cross-correlation may be realizable in a proximity induced NW where the length of the superconducting region can be $L = 0.75\xi \sim 5 - 15$ nm. Our setup may also be used for making future generation entangler devices with unconventional superconductor^{7,19,47}.

ACKNOWLEDGMENTS

We acknowledge Arun M. Jayannavar for valuable discussions.

Appendix: Expression for the shot noise

We study the current cross-correlation in our NSN geometry at zero temperature and zero frequency limit following⁴⁰. The shot noise contributions arising from different scattering amplitudes can be separated in terms of the normal reflection, AR, CT and CAR amplitudes as follows.

$$\begin{aligned} S_{ij}^{ee}(\epsilon) &= -\frac{2e^2}{h}[(t_e(\epsilon)r_e^*(\epsilon) + r_e(\epsilon)t_e^*(\epsilon))^2 \\ &\quad + (t_h(\epsilon)r_h^*(\epsilon) + r_h(\epsilon)t_h^*(\epsilon))^2], \\ S_{ij}^{eh}(\epsilon) &= \frac{4e^2}{h}|r_h(\epsilon)t_e^*(\epsilon) + t_h(\epsilon)r_e^*(\epsilon)|^2. \end{aligned} \quad (\text{A.1})$$

Hence the total shot noise reads,

$$S_{ij}(\epsilon) = S_{ij}^{ee}(\epsilon) + S_{ij}^{eh}(\epsilon) \quad (\text{A.2})$$

where, S_{ij}^{ee} , S_{ij}^{eh} represent the cross-correlation corresponding to the phenomenon of CT and CAR respectively. Also, due to particle-hole symmetry we can write

$$\begin{aligned} S_{ij}^{ee}(\epsilon) &= S_{ij}^{hh}(\epsilon) \\ S_{ij}^{eh}(\epsilon) &= S_{ij}^{he}(\epsilon). \end{aligned} \quad (\text{A.3})$$

Here we scale r_h and t_h by $\sqrt{\frac{k_h}{k_e}}$ (*i.e.* after scaling we have $r_h \equiv r_h \sqrt{\frac{k_h}{k_e}}$ and $t_h \equiv t_h \sqrt{\frac{k_h}{k_e}}$) in order to maintain the probability conservation (unitarity) as discussed earlier. All these scattering amplitudes are complex and hence they can be expressed as follow,

$$\begin{aligned} r_h &= |r_h|e^{i\theta_1}, & r_e &= |r_e|e^{i\theta_2} \\ t_h &= |t_h|e^{i\phi_1}, & t_e &= |t_e|e^{i\phi_2} \end{aligned}$$

where θ_1 , θ_2 , ϕ_1 , ϕ_2 are the phase factors of the corresponding complex scattering amplitudes. They play crucial role in determining the nature of the shot noise which can be realized from Eq. (A.1). We emphasize the scenario where all the scattering probabilities are equal in magnitude (0.25) *i.e.* the zero energy resonance condition. As mentioned earlier, we obtain this zero energy resonance for both undoped ($\mu = 0$) and doped ($\mu \neq 0$) condition. This, at zero energy, the expression for shot noise cross-correlation takes the form,

$$\begin{aligned} S_{ij}(\epsilon) &= -\frac{e^2}{2h}[\cos^2(\phi_2 - \theta_2) + \cos^2(\phi_1 - \theta_1)] \\ &\quad + \frac{e^2}{2h}[1 + \cos(\theta_1 + \theta_2 - \phi_1 - \phi_2)]. \end{aligned} \quad (\text{A.4})$$

From Eq. (A.4) it is evident that shot-noise correlation depends only on the phases of different scattering amplitudes at resonance. If the phases cancel out among each other then S_{ij} becomes zero which we obtain at the resonance.

^{*} ganeshpaul@iopb.res.in

[†] paramitad@iopb.res.in; First two authors have contributed equally to this work.

[‡] arijit@iopb.res.in

¹ G. Blonder, M. Tinkham, and T. M. Klapwijk, *Phys. Rev. B* **25**, 4515 (1982).

² T. Klapwijk, *J. superconductivity* **17**, 593 (2004).

³ A. Saha, *Int. J. Mod. Phys. B* **27**, 1330015 (2013).

⁴ A. Andreev, *Zh. Ekspерим. i Teor. Fiz.* **46** (1964).

⁵ G. Falci, D. Feinberg, and F. Hekking, *Europhys. Lett.* **54**, 255 (2001).

⁶ G. Bignon, M. Houzet, F. Pistolesi, and F. W. J. Hekking, *Europhys. Lett.* **67**, 110 (2004).

⁷ P. Recher, E. V. Sukhorukov, and D. Loss, *Phys. Rev. B* **63**, 165314 (2001).

⁸ J. P. Morten, A. Brataas, and W. Belzig, *Phys. Rev. B* **74**, 214510 (2006).

⁹ A. L. Yeyati, F. S. Bergeret, A. Martin-Rodero, and T. M. Klapwijk, *Nat. Phys.* **3**, 455 (2007).

¹⁰ S. Das, S. Rao, and A. Saha, *Europhys. Lett.* **81**, 67001 (2008).

¹¹ S. Russo, M. Kroug, T. Klapwijk, and A. Morpurgo, *Phys. Rev. Lett.* **95**, 027002 (2005).

¹² P. C. Zimansky and V. Chandrasekhar, *Phys. Rev. Lett.* **97**, 237003 (2006).

¹³ J. Wei and V. Chandrasekhar, *Nat. Phys.* **4**, 494 (2010).

¹⁴ A. Das, Y. Ronen, M. Heiblum, D. Mahalu, A. V. Kretinin, and H. Shtrikman, *Nat. Commun.* **3**, 1165 (2012).

¹⁵ L. Hofstetter, S. Csonka, J. Nygård, and C. Schönenberger, *Nature* **461**, 960 (2009).

¹⁶ L. G. Herrmann, F. Portier, P. Roche, A. Levy Yeyati, T. Kontos, and C. Strunk, *Phys. Rev. Lett.* **104**, 026801 (2010).

¹⁷ P. C. Zimansky, J. Wei, and V. Chandrasekhar, *Nat. Phys.* **5**, 393 (2009).

¹⁸ J. Brauer, F. Hübner, M. Smetanin, D. Beckmann, and H. v. Löhneysen, *Phys. Rev. B* **81**, 024515 (2010).

¹⁹ G. B. Lesovik, T. Martin, and G. Blatter, *Eur. Phys. J. B* **24**, 287 (2001).

²⁰ M. Yamashiro, Y. Tanaka, Y. Tanuma, and S. Kashiwaya, *J. Phys. Soc. Japan* **67**, 3224 (1998).

²¹ C. Honerkamp and M. Sigrist, *J. Low Temp. Phys.* **111**, 895 (1998).

²² K. Sengupta, R. Roy, and M. Maiti, *Phys. Rev. B* **74**, 094505 (2006).

²³ S. Yip, *Annu. Rev. Condens. Matter Phys.* **5**, 15 (2014).

²⁴ E. Bauer and M. Sigrist, *Non-centrosymmetric superconductors: introduction and overview*, Vol. 847 (Springer Science & Business Media, 2012).

²⁵ Y. Yanase and M. Sigrist, *J. Phys. Soc. Japan* **77**, 124711 (2008).

²⁶ M. Nishiyama, Y. Inada, and G. Zheng, *Phys. Rev. Lett.* **98**, 047002 (2007).

²⁷ M. Sigrist and K. Ueda, *Rev. Mod. Phys.* **63**, 239 (1991).

²⁸ Y. Tanaka, M. Sato, and N. Nagaosa, *J. Phys. Soc. Japan* **81**, 011013 (2011).

²⁹ P. Frigeri, D. Agterberg, A. Koga, and M. Sigrist, *Phys. Rev. Lett.* **92**, 097001 (2004).

³⁰ P. Burset, F. Keidel, Y. Tanaka, N. Nagaosa, and B. Trauzettel, *Phys. Rev. B* **90**, 085438 (2014).

³¹ Y. Tanaka, T. Yokoyama, A. V. Balatsky, and N. Nagaosa, *Phys. Rev. B* **79**, 060505(R) (2009).

³² C. K. Lu and S. Yip, *Phys. Rev. B* **82**, 104501 (2010).

³³ A. Karki, Y. Xiong, I. Vekhter, D. Browne, P. Adams, D. Young, K. Thomas, J. Y. Chan, H. Kim, and R. Prozorov, *Phys. Rev. B* **82**, 064512 (2010).

³⁴ M. Sato and S. Fujimoto, *Phys. Rev. B* **79**, 094504 (2009).

³⁵ L. Santos, T. Neupert, C. Chamon, and C. Mudry, *Phys. Rev. B* **81**, 184502 (2010).

³⁶ M. Duckheim and P. W. Brouwer, *Phys. Rev. B* **83**, 054513 (2011).

³⁷ A. Kundu, S. Rao, and A. Saha, *Europhys. Lett.* **88**, 57003 (2009).

³⁸ Y. M. Blanter and M. Büttiker, *Phys. Rep.* **336**, 1 (2000).

³⁹ C. W. J. Beenakker and C. Schönenberger, *Phys. Today* **56**, 37 (2003).

⁴⁰ M. Anantram and S. Datta, *Phys. Rev. B* **53**, 16390 (1996).

⁴¹ D. Chevallier, J. Rech, T. Jonckheere, and T. Martin, *Phys. Rev. B* **83**, 125421 (2011).

⁴² J. Rech, D. Chevallier, T. Jonckheere, and T. Martin, *Phys. Rev. B* **85**, 035419 (2012).

⁴³ A. Haim, E. Berg, F. von Oppen, and Y. Oreg, *Phys. Rev. Lett.* **114**, 166406 (2015).

⁴⁴ A. Haim, E. Berg, F. von Oppen, and Y. Oreg, *Phys. Rev. B* **92**, 245112 (2015).

⁴⁵ K. M. Tripathi, S. Das, and S. Rao, *Phys. Rev. Lett.* **116**, 166401 (2016).

⁴⁶ M. Mondal, B. Joshi, S. Kumar, A. Kamlapure, S. C. Ganguli, A. Thamizhavel, S. S. Mandal, S. Ramakrishnan, and P. Raychaudhuri, *Phys. Rev. B* **86**, 094520 (2012).

⁴⁷ R. P. Tiwari, W. Belzig, M. Sigrist, and C. Bruder, *Phys. Rev. B* **89**, 184512 (2014).